Journal of Computational Physics 421 (2020) 109729

Contents lists available at ScienceDirect

Journal of Computational Physics

www.elsevier.com/locate/jcp

Conservative discontinuous Galerkin methods for the nonlinear Serre equations

Jianli Zhao [a], Qian Zhang [a,1,2], Yang Yang [b,3], Yinhua Xia [a,*,4]

[a] School of Mathematical Sciences, University of Science and Technology of China, Hefei, Anhui 230026, PR China
[b] Department of Mathematical Sciences, Michigan Technological University, Houghton, MI 49931, USA

ARTICLE INFO

Article history:
Received 10 January 2020
Received in revised form 17 July 2020
Accepted 19 July 2020
Available online 24 July 2020

Keywords:
Serre equations
Discontinuous Galerkin methods
Conservative schemes
Well-balanced schemes

ABSTRACT

In this paper, we develop three conservative discontinuous Galerkin (DG) schemes for the one-dimensional nonlinear dispersive Serre equations, including two conserved schemes for the equations in conservative form and a Hamiltonian conserved scheme for the equations in non-conservative form. One of the schemes owns the well-balanced property via constructing a high order approximation to the source term for the Serre equations with a non-flat bottom topography. By virtue of the Hamiltonian structure of the Serre equations, we introduce an Hamiltonian invariant and then develop a DG scheme which can preserve the discrete version of such an invariant. Numerical experiments in different cases are performed to verify the accuracy and capability of these DG schemes for solving the Serre equations.

1. Introduction

We introduce and study the discontinuous Galerkin (DG) methods for the Serre equations

$$\begin{cases} h_t + (hu)_x = 0, \\ u_t + uu_x + gh_x + \beta h^{-1}(h^2\gamma)_x = 0, \\ \gamma = h(u_x{}^2 - u_{xt} - uu_{xx}), \end{cases} \tag{1.1}$$

where $h(x,t)$ represents the total water depth, $u(x,t)$ is the averaged velocity of the fluid, g is the gravitational constant, β is a parameter and γ is the fluid vertical acceleration on the free surface.

The Serre equations (1.1) can be used to describe the shallow water with large amplitude on the free surface. In [40], we know that Euler equations of the incompressible fluid flow describe the propagation of the full water waves on the free surface. Since the difficulty in solving this problem is mainly caused by the free surface, various approximate models for this case are presented, and the corresponding analytical theories and numerical simulations are also developed. In these

* Corresponding author.
E-mail addresses: zjl88914@mail.ustc.edu.cn (J. Zhao), gelee@mail.ustc.edu.cn, qian77.zhang@polyu.edu.hk (Q. Zhang), yyang7@mtu.edu (Y. Yang), yhxia@ustc.edu.cn (Y. Xia).
[1] Current address: Department of Applied Mathematics, The Hong Kong Polytechnic University, Hong Kong.
[2] Research supported by the 2019 Hong Kong Scholar Program.
[3] Research supported by NSF grant DMS-1818467.
[4] Research supported by National Numerical Windtunnel grant NNW2019ZT4-B08 and NSFC grant No. 11871449.

https://doi.org/10.1016/j.jcp.2020.109729
0021-9991/

models, the propagation of the waves under the assumption of shallow water with large amplitude is governed by the Serre equations, while for small amplitude or weakly nonlinear shallow water waves the model reduces to the classical Boussinesq system [40]. The Serre equations can be regarded as an asymptotic approximation of the two-dimensional Euler equations. It is a fully nonlinear dispersive system that models two-way propagation of long waves on the surface of an ideal fluid in a channel. And if we ignore all the dispersive terms, it will become a hyperbolic system of shallow water wave. The dispersive terms combined by the temporal and spatial derivatives are the major difficulty in solving the Serre equations [16].

The Serre equations were first derived by Francois Serre [36] in 1953 and then restudied by Su and Gardner [39], Green [22], Seabra-Santos et al. [35], Green and Naghdi in [23] derived the system with two spatial dimensions for general uneven bottoms in 1976. Lannes and Bonneton in [24] provided the formal derivation of the equations from Euler equations and the justification for several approximative water wave models of Euler equations. Further studies can be got from some recent literatures by Barthélemy [3], Dias and Milewski [16], Carter and Cienfuegos [9], and the references therein.

There are various numerical methods dealing with the nonlinear Serre equations including higher order dispersive terms. In [26], a pseudo-spectral method was proposed and used to solve the one-dimensional Serre equations for free surface waves in a homogeneous layer of an ideal fluid. In [29,7,8,2,18], finite difference and finite volume methods were also applied in simulating all the processes of wave transformation with nonlinear dispersive effect. For the equations with non-flat bottoms (Green-Naghdi equations), the well-balanced central DG method was proposed in [25], in which the elliptic part was solved by the continuous finite element method. A local DG (LDG) scheme was presented in [31] for the one-dimensional Green-Naghdi equations based on rotational characteristics in the velocity field. For the two-dimensional problem, Duran and Marche developed a LDG method by rewriting the equations as a hyperbolic-elliptic system in [17], and a hybridized DG method was introduced in [34] for the splitting system (the hyperbolic part and dispersive part). As for the shallow water equations and other hyperbolic conservation laws, the conservative scheme is demanded when the solution is not smooth enough. In this paper, we will develop the LDG methods for the Serre equations based on their conservation laws and also well-balanced property as in the shallow water equations.

The DG method which is a class of finite element methods was first introduced by Reed and Hill [33] for solving the neutron transport linear equation in 1973. Completely discontinuous piecewise polynomial space is used for the test functions and the numerical solutions in this method. Later, Cockburn and Shu have made a great contribution in developing the DG method in a series of papers [11,13–15]. They used the stable high order Runge-Kutta methods for temporal discretization and the exact or approximate Riemann solvers as the interface fluxes in spatial discretization. In addition, they also designed the LDG method for solving convection-diffusion problems containing second derivative terms, which was motivated by Bassi and Rebay [4] in solving the compressible Navier-Stokes equations. At present, the DG method is widely used in many areas, such as gas dynamics, electromagnetism, magnetohydrodynamics, modeling of shallow water, etc. Moreover, the DG method enjoys many attractive properties. First we can get high order accuracy for the numerical solution by using element-based test functions. Second the DG method can be applied on arbitrary unstructured meshes with the suitable choices of the interelement boundary fluxes. Finally, parallel computing can easily be applied due to local data communications. In addition to the advantages given above, the LDG method contains auxiliary variables that approximate the gradients of the primary solutions to the expected order of accuracy. Then the auxiliary variables can be locally eliminated. The LDG methods have been generalized to nonlinear wave equations in [49,50,43–47,51], such as KdV equation, Camassa-Holm equation and nonlinear Schrödinger equation, etc. We refer to the review paper [48] of LDG methods for high-order time-dependent partial differential equations and the references therein.

Most recently, a series of schemes so called structure-preserving schemes for nonlinear wave equations have been attracted considerable attention. For some integrable equations, such as KdV type equations [6,27,52,53], Zakharov system [42], Schrödinger-KdV system [41], etc., the authors proposed various conservative numerical schemes to “preserve the structures”. For the Serre equations, the aliasing or spurious dissipative effects will result in significant errors for solving large amplitude or rapidly oscillating waves, such as the dispersive shock waves. Therefore, Mitsotakis and Dutykh [30] constructed a non-dissipative finite element method to approximate the rapidly oscillating waves accurately. A fundamental property of the Serre equations is its Hamiltonian structure. From the following conservation laws derived by the equations (1.1),

$$(hu)_t + (hu^2 + \frac{1}{2}gh^2 + \beta h^2\gamma)_x = 0, \tag{1.2}$$

$$(hu - \beta(h^3u_x)_x)_t + (hu^2 + \frac{1}{2}gh^2 - 2\beta h^3u_x^2 - \beta h^3uu_{xx} - 3\beta h^2h_xuu_x)_x = 0, \tag{1.3}$$

$$(u - \beta h^{-1}(h^3u_x)_x)_t + (\frac{1}{2}u^2 + gh - \frac{1}{2}h^2u_x^2 - \beta uh^{-1}(h^3u_x)_x)_x = 0, \tag{1.4}$$

$$(\frac{1}{2}hu^2 + \frac{1}{2}\beta h^3u_x^2 + \frac{1}{2}gh^2)_t + ((\frac{1}{2}u^2 + \frac{1}{2}\beta h^2u_x^2 + gh + \beta h\gamma)hu)_x = 0, \tag{1.5}$$

we have the corresponding conservative quantities E_0, E_1, E_2 and Hamiltonian $\mathcal{H}$ in the relevant domain I,

$$E_0 = \int_I hudx,$$

$$E_1 = \int_I (hu - \beta(h^3 u_x)_x)dx,$$

$$E_2 = \int_I (u - \beta h^{-1}(h^3 u_x)_x)dx,$$

$$\mathcal{H} = \int_I \frac{1}{2}(hu^2 + \beta h^3 u_x^2 + gh^2)dx.$$

The numerical schemes can be established based on the above conserved quantities. For the form (1.2), the main difficulty in designing E_0 conserved numerical scheme lies in the mixed spatial and temporal derivatives in γ. Therefore, we design and implement three kinds of numerical schemes which are all based on the DG methods for the one-dimensional Serre equations. The first two are constructed for E_1 and E_2 in the conservative form, and the last one preserves the Hamiltonian invariant $\mathcal{H}$ in a non-conservative form. The E_1 conserved scheme can maintain the still-water stationary for the water wave equations over non-flat bottom topography, so called well-balanced scheme. For the Hamiltonian ($\mathcal{H}$) conserved DG scheme, we take advantage of the DG method for Hamilton-Jacobi equations [10] to deal with the nonlinear terms. Moreover, the stability of the Hamiltonian for the Serre equations would be proved theoretically.

The present paper is organized as follows. In Section 2, the E_1 and E_2 conserved DG schemes are designed in detail. For the E_1 conserved scheme, we also discuss and prove its well-balanced property when the bottom is not flat. Section 3 is devoted to elaborate the Hamiltonian ($\mathcal{H}$) conserved DG scheme. Moreover, the stability based on the Hamiltonian is also given in this part. In Section 4, numerical experiments in different circumstances are provided to illustrate the accuracy and capability of these schemes. Concluding remarks are given in Section 5.

2. The LDG discretization in conservative form

In this section, we devote to design LDG schemes for the Serre equations by adopting the conservation laws E_1 and E_2 in (1.3) and (1.4) respectively, and then give the corresponding algorithm flowcharts.

To discretize the spatial derivatives, we proceed as follows. For each partition of the interval $I = [a, b]$, we set the cells and cell centers as $I_j = [x_{j-\frac{1}{2}}, x_{j+\frac{1}{2}}]$, $x_j = \frac{1}{2}(x_{j-\frac{1}{2}} + x_{j+\frac{1}{2}})$ for $j = 1, \cdots, N$, and denote the mesh size $\Delta x = \max_{1\le j\le N} \Delta x_j$ with $\Delta x_j = x_{j+\frac{1}{2}} - x_{j-\frac{1}{2}}$. The mesh is assumed to be quasi-uniform, namely there exists a positive constant c such that $\Delta x \le c \min_{1\le j\le N} \Delta x_j$.

We seek the numerical approximations belonging to the finite element space

$$V_h = \{v(x) : v(x) \in P^k(I_j) \text{ for } x \in I_j, \quad j = 1, \cdots, N\},$$

where $P^k(I_j)$ denotes polynomials in I_j of degree up to k. It transpires that the functions belonging to V_h could be discontinuous across the cell interfaces. For $v \in V_h$, the values of v at $x_{j+\frac{1}{2}}$, from the left and right cells I_j and I_{j+1}, can be regarded as $v^-_{j+\frac{1}{2}}$ and $v^+_{j+\frac{1}{2}}$, respectively. The notations $[\![v]\!] = v^+ - v^-$ and $\{\!\{v\}\!\} = \frac{1}{2}(v^+ + v^-)$ are used to represent the jump and the mean of the function at the cell interfaces.

2.1. E_1 conserved DG scheme

In order to treat the mixed spatial and temporal derivatives in (1.1), we adopt the conservation law (1.3) and develop the E_1 conserved DG scheme for the following system

$$h_t + (hu)_x = 0, \tag{2.1a}$$

$$z_t + (uz + \frac{1}{2}gh^2 - 2\beta h^3 q^2)_x = 0, \tag{2.1b}$$

$$hu - \beta(h^3 q)_x = z, \tag{2.1c}$$

$$q - u_x = 0, \tag{2.1d}$$

with periodic boundary conditions. To design the LDG method, we accomplish the complete schemes for the system as follows. For simplicity, we still use h, u, z and q to denote the numerical solutions.

For the time-dependent equations (2.1a) and (2.1b), assume that u and q are known and h and z are to be solved, then we can formulate the DG method as follows: Find $h, z \in V_h$ such that, for all test functions $\theta, \varphi \in V_h$,

$$\int_{I_j} h_t \theta dx - \int_{I_j} (hu)\theta_x dx + (\widehat{f}_1 \theta^-)_{j+\frac{1}{2}} - (\widehat{f}_1 \theta^+)_{j-\frac{1}{2}} = 0, \tag{2.2}$$

$$\int_{I_j} z_t \varphi dx - \int_{I_j} (uz + \frac{1}{2}gh^2 - 2\beta h^3 q^2)\varphi_x dx + (\widehat{f_2}\varphi^-)_{j+\frac{1}{2}} - (\widehat{f_2}\varphi^+)_{j-\frac{1}{2}} = 0, \tag{2.3}$$

$\forall j = 1, \cdots, N$. The "hat" terms $\widehat{f_1}$ and $\widehat{f_2}$ appear on the cell boundary terms are the so-called numerical fluxes, which are single valued functions from integration by parts and should be designed to ensure the stability of the schemes. For conservation laws, the numerical fluxes are usually Lipschitz continuous functions and preserve the monotone property and consistent property, named the monotone fluxes [12]. Here, we can choose the following dissipative numerical flux

$$\widehat{f_1} = \{\!\{hu\}\!\} - \frac{\alpha}{2}[\![h]\!], \tag{2.4}$$

$$\widehat{f_2} = \{\!\{uz + \frac{1}{2}gh^2 - 2\beta h^3 q^2\}\!\} - \frac{\alpha}{2}[\![z]\!], \tag{2.5}$$

where $\alpha = \max(|u| + \sqrt{gh})$ is the maximum taken in the relevant interval. We have omitted the half-integer indices $j + \frac{1}{2}$ as all quantities in (2.4) are computed at the same cell interfaces.

For the time-independent equations (2.1c) and (2.1d), assume that h and z are known and u and q are to be solved, the LDG scheme can be formulated as follows: Find $u, q \in V_h$ such that, for all test functions $\rho, \phi \in V_h$,

$$\int_{I_j} hu\rho dx + \int_{I_j} \beta h^3 q \rho_x dx - (\widehat{h^3 q}\rho^-)_{j+\frac{1}{2}} + (\widehat{h^3 q}\rho^+)_{j-\frac{1}{2}} = \int_{I_j} z\rho dx, \tag{2.6a}$$

$$\int_{I_j} q\phi dx + \int_{I_j} u\phi_x dx - (\widehat{u}\phi^-)_{j+\frac{1}{2}} + (\widehat{u}\phi^+)_{j-\frac{1}{2}} = 0. \tag{2.6b}$$

Here we take the alternating fluxes [48] such as

$$\widehat{h^3 q} = (h^3 q)^-, \quad \widehat{u} = u^+. \tag{2.7}$$

2.1.1. Algorithm flowchart (I)

This part shows the implementation about the fully-discrete E_1 conserved scheme. For simplicity, we choose the Euler forward method to illustrate the numerical evolution from time level t^n to time level t^{n+1}. In numerical experiments, the explicit SSP/TVD Runge-Kutta methods [37,38] are adopted, which can be viewed as the convex combinations of the Euler forward method.

Let $\mathbf{h}, \mathbf{u}, \mathbf{z}$ and $\mathbf{q}$ denote the vectors containing the degrees of freedom for the numerical solutions h, u, z and q, respectively. Given the solution $\mathbf{h^n}, \mathbf{u^n}, \mathbf{z^n}$ and $\mathbf{q^n}$ at the time level t^n, the algorithm can be divided into two steps.

Step I: From the equations (2.2) and (2.3) equipped with the corresponding numerical fluxes (2.4) and (2.5), we have the fully discrete scheme in the matrix form:

$$\frac{\mathbf{h^{n+1}} - \mathbf{h^n}}{\Delta t^n} = \mathbf{res_1}(\mathbf{h^n}, \mathbf{u^n}), \tag{2.8}$$

$$\frac{\mathbf{z^{n+1}} - \mathbf{z^n}}{\Delta t^n} = \mathbf{res_2}(\mathbf{h^n}, \mathbf{u^n}, \mathbf{z^n}, \mathbf{q^n}), \tag{2.9}$$

by the Euler forward method with the time step $\Delta t^n = t^{n+1} - t^n$.

Step II: After we get $\mathbf{h^{n+1}}$ and $\mathbf{z^{n+1}}$ from the above, based on the schemes (2.6a) and (2.6b) with the fluxes (2.7), we can solve $\mathbf{u^{n+1}}, \mathbf{q^{n+1}}$ in the following matrix form

$$\mathbf{A}(\mathbf{h^{n+1}})\mathbf{u^{n+1}} + \mathbf{B}(\mathbf{h^{n+1}})\mathbf{q^{n+1}} = \mathbf{z^{n+1}}, \tag{2.10}$$

$$\mathbf{q^{n+1}} + \mathbf{C}\mathbf{u^{n+1}} = 0, \tag{2.11}$$

where the matrices $\mathbf{A}$, $\mathbf{B}$ and $\mathbf{C}$ are the corresponding discrete operators in the scheme. Then we get all the numerical solutions at time level t^{n+1}.

2.1.2. The well-balanced scheme

In this subsection, we turn to present the well-balanced property of E_1 conserved DG scheme for the Serre equations with a non-flat bottom, also known as Green and Naghdi equations in [23]. Thereinto, h can be represented as the sum of d and η, where d denotes the bottom topography and η is the free surface elevation. In consideration of the one-dimensional shallow water flows with non-flat bottom topography, the model can be formulated as follows:

$$h_t + (hu)_x = 0, \tag{2.12a}$$

$$(hu)_t + (hu^2 + \frac{1}{2}gh^2 + \beta h^2\gamma + \frac{1}{2}h^2\Psi)_x = (gh + \frac{1}{2}h\gamma + h\Psi)d_x, \tag{2.12b}$$

with

$$\Psi = -d_x u_t - d_x u u_x - d_{xx}u^2. \tag{2.13}$$

It can be seen that for the flat bottom, meaning $d(x)$ is a constant, the equation (2.12b) is equivalent to the equation (1.2).

The well-balanced methods [5] are introduced to exactly preserve the still-water stationary solution at a discrete level. For the Serre equations, the still-water stationary wave solution can be represented as follows,

$$u = 0 \quad \text{and} \quad \eta = h - d = constant. \tag{2.14}$$

In order to deal with the mixed spatial and temporal derivatives in (2.12b), we introduce a new unknown variable

$$\omega = -\beta(h^3 u_x)_x + h(1 - h_x d_x - \frac{1}{2}hd_{xx} + d_x^2)u. \tag{2.15}$$

Notice that $\omega = z$ with the flat bottom. The equation (2.15) can be discretized similarly as the LDG scheme (2.6a) and (2.6b) for z. Thus we omit the details here.

As in [25], we rewrite the time-dependent part of the system (2.12a)–(2.12b) into a balance law

$$\eta_t + (hu)_x = 0, \tag{2.16}$$

$$\omega_t + (\omega u + \frac{1}{2}gh^2 - 2\beta h^3 u_x^2 - h^2 u u_x d_x)_x = ghd_x + \frac{1}{2}h^2 u u_x d_{xx} + hu^2 d_x d_{xx}. \tag{2.17}$$

Denoting $U = (\eta, \omega)^T$ as the unknowns, we formulate the E_1 conserved scheme for the balance equations as follows: Find $\eta, \omega \in V_h$ such that, for all test functions $\theta_1, \theta_2 \in V_h$,

$$\int_{I_j} U_t \cdot \Theta dx - \int_{I_j} F \cdot \Theta_x dx + (\widehat{F} \cdot \Theta^-)_{j+\frac{1}{2}} - (\widehat{F} \cdot \Theta^+)_{j-\frac{1}{2}} = \int_{I_j} S \cdot \Theta dx, \quad \forall j = 1, \cdots, N, \tag{2.18}$$

where Θ equals $(\theta_1, \theta_2)^T$, the flux is taken as

$$F(U) = (hu, \omega u + \frac{1}{2}gh^2 - 2\beta h^3 u_x^2 - h^2 u u_x d_x)^T,$$

and the source term is given by

$$S = (0, ghd_x + \frac{1}{2}h^2 u u_x d_{xx} + hu^2 d_x d_{xx})^T.$$

In general, the numerical scheme (2.18) does not have the well-balanced property. Based on the idea in [32], we discretize the source term as follows:

$$\int_{I_j} U_t \cdot \Theta dx - \int_{I_j} F \cdot \Theta_x dx + (\widehat{F} \cdot \Theta^-)_{j+\frac{1}{2}} - (\widehat{F} \cdot \Theta^+)_{j-\frac{1}{2}} = \int_{I_j} S_1 \cdot \Theta dx + \widetilde{S}_j, \tag{2.19}$$

with

$$S_1 = (0, \frac{1}{2}h^2 u u_x d_{xx} + hu^2 d_x d_{xx})^T,$$

and

$$\begin{aligned}
&\widetilde{S}_j = (0, \tilde{s}_j)^T, \\
&\tilde{s}_j = \frac{1}{2}g(-\int_{I_j} d^2(\theta_2)_x dx + \{\!\{d^2_{j+\frac{1}{2}}\}\!\}(\theta_2)^-_{j+\frac{1}{2}} - \{\!\{d^2_{j-\frac{1}{2}}\}\!\}(\theta_2)^+_{j-\frac{1}{2}}) \\
&\quad + g\bar{\eta}_j(-\int_{I_j} d(\theta_2)_x dx + \{\!\{d_{j+\frac{1}{2}}\}\!\}(\theta_2)^-_{j+\frac{1}{2}} - \{\!\{d_{j-\frac{1}{2}}\}\!\}(\theta_2)^+_{j-\frac{1}{2}}) \\
&\quad + \int_{I_j} g(\eta - \bar{\eta}_j)d_x\theta_2 dx,
\end{aligned} \tag{2.20}$$

where $\tilde{s}_j$ is the high order approximation of the source term $\int_{I_j} ghd_x\theta_2 dx$ and $\bar{\eta}_j = \frac{1}{|I_j|}\int_{I_j}\eta dx$ denotes the mean of η over I_j. $\widehat{F}$ is a monotone flux, e.g. the Lax-Friedrichs flux.

In order to ensure the unique solvability of the equation (2.15) in the still-water stationary, the following assumptions are needed [25]:

(A1) The water height h in the still-water stationary solution considered here has a strictly positive lower bound.
(A2) $1 - \frac{1}{2}hd_{xx} > 0$.

Now we turn to prove the well-balanced property of the modified scheme (2.19).

Proposition 2.1. *(Well-balanced property) Under the assumptions (A1) and (A2), the modified E_1 conserved DG scheme described by (2.19) for the Serre equations with non-flat bottom has the well-balanced property.*

Proof. Let U^n $(n \in \mathbb{N})$ be the numerical solution of (2.19) at time level t^n. For brevity, here we consider Euler forward time discretization, which can be easily generalized to the SSP/TVD Runge-Kutta methods. Then we apply them into (2.19), leading to

$$\int_{I_j} U^{n+1}\cdot\Theta dx = \int_{I_j} U^n\cdot\Theta dx + \Delta t^n\Big(\int_{I_j} F^n\cdot\Theta_x dx - (\widehat{F^n}\cdot\Theta^-)_{j+\frac{1}{2}} + (\widehat{F^n}\cdot\Theta^+)_{j-\frac{1}{2}} + \int_{I_j} S_1^n\cdot\Theta dx + (\widetilde{S^n})_j\Big). \tag{2.21}$$

By induction, first we assume

$$U^n = (C_0, 0)^T \quad \text{and} \quad u^n = 0, \tag{2.22}$$

where C_0 is a constant. From this assumption we want to deduce that the numerical solution computed from (2.21) satisfies

$$U^{n+1} = (C_0, 0)^T \quad \text{and} \quad u^{n+1} = 0. \tag{2.23}$$

By virtue of the assumptions (2.22), the equation (2.21) becomes

$$\eta^{n+1} = \eta^n = C_0, \tag{2.24}$$

$$\int_{I_j}\omega^{n+1}\theta_2 dx = \Delta t^n\Big(\int_{I_j}\frac{1}{2}g(h^n)^2(\theta_2)_x dx - (\frac{1}{2}g\{\!\{(h^n)^2\}\!\}(\theta_2)^-)_{j+\frac{1}{2}} + (\frac{1}{2}g\{\!\{(h^n)^2\}\!\}(\theta_2)^+)_{j-\frac{1}{2}} + (\widetilde{s^n})_j\Big). \tag{2.25}$$

Denoting the sum of the right-hand side of equation ((2.25)) by R_j, we can get

$$\begin{aligned}
R_j &= \Delta t^n\Big(\int_{I_j}\frac{1}{2}g(h^n)^2(\theta_2)_x dx - (\frac{1}{2}g\{\!\{(h^n)^2\}\!\}(\theta_2)^-)_{j+\frac{1}{2}} + (\frac{1}{2}g\{\!\{(h^n)^2\}\!\}(\theta_2)^+)_{j-\frac{1}{2}} + (\widetilde{s^n})_j\Big)\\
&= \Delta t^n\Big(\int_{I_j}\frac{1}{2}g((h^n)^2 - (d^n)^2 - 2\bar{\eta}_j^n d^n)(\theta_2)_x dx - \frac{1}{2}g(\{\!\{(h^n)^2_{j+\frac{1}{2}}\}\!\} - \{\!\{(d^n)^2_{j+\frac{1}{2}}\}\!\} - 2\bar{\eta}_j^n\{\!\{d^n_{j+\frac{1}{2}}\}\!\})(\theta_2)^-_{j+\frac{1}{2}}\\
&\quad + \frac{1}{2}g(\{\!\{(h^n)^2_{j-\frac{1}{2}}\}\!\} - \{\!\{(d^n)^2_{j-\frac{1}{2}}\}\!\} - 2\bar{\eta}_j^n\{\!\{d^n_{j-\frac{1}{2}}\}\!\})(\theta_2)^+_{j-\frac{1}{2}} + \int_{I_j} g(\eta^n - \bar{\eta}_j^n)d_x^n\theta_2 dx\Big)\\
&= \Delta t^n\Big(\int_{I_j}\frac{1}{2}g(\eta^n)^2(\theta_2)_x dx - \frac{1}{2}g\{\!\{(\eta^n)^2_{j+\frac{1}{2}}\}\!\}(\theta_2)^-_{j+\frac{1}{2}} + \frac{1}{2}g\{\!\{(\eta^n)^2_{j-\frac{1}{2}}\}\!\}(\theta_2)^+_{j-\frac{1}{2}}\Big)\\
&= 0,
\end{aligned} \tag{2.26}$$

where we take use of the relationship $h = d + \eta$ and the fact $\eta^n = \bar{\eta}_j^n = C_0$ by (2.22). Then the equations (2.24)–(2.25) lead to $U^{n+1} = (C_0, 0)^T$. As the assumptions (A1) and (A2) ensure the unique solvability of the finite element discretization, it implies $u^{n+1} = 0$. This completes our proof. □

2.2. E_2 conserved DG scheme

Similar to the development of the E_1 conserved scheme, we adopt (1.1) and (1.4) to construct the E_2 conserved scheme. The Serre equations are rewritten as follows:

$$h_t + (hu)_x = 0, \tag{2.27a}$$

$$\widetilde{z}_t + (u\widetilde{z} - \frac{1}{2}u^2 + gh - \frac{1}{2}h^2q^2)_x = 0, \tag{2.27b}$$

$$u - h^{-1}p = \widetilde{z}, \tag{2.27c}$$

$$p - \beta(h^3q)_x = 0, \tag{2.27d}$$

$$q - u_x = 0. \tag{2.27e}$$

Without ambiguity, we still use $h, \widetilde{z}, u, p, q$ to denote the numerical approximations. The E_2 conserved DG scheme for (2.27a)-(2.27e) can be formulated as follows: Find $h, u, q, \widetilde{z}, p \in V_h$, such that, for all test functions θ, φ, ρ, ψ and $\phi \in V_h$,

$$\int_{I_j} h_t\theta dx - \int_{I_j} (hu)\theta_x dx + (\widehat{f}_1\theta^-)_{j+\frac{1}{2}} - (\widehat{f}_1\theta^+)_{j-\frac{1}{2}} = 0, \tag{2.28}$$

$$\int_{I_j} \widetilde{z}_t\varphi dx - \int_{I_j} (u\widetilde{z} - \frac{1}{2}u^2 + gh - \frac{1}{2}h^2q^2)\varphi_x dx + (\widehat{f}_4\varphi^-)_{j+\frac{1}{2}} - (\widehat{f}_4\varphi^+)_{j-\frac{1}{2}} = 0, \tag{2.29}$$

$$\int_{I_j} p\rho dx + \int_{I_j} \beta h^3 q\rho_x dx - (\widehat{h^3q}\rho^-)_{j+\frac{1}{2}} + (\widehat{h^3q}\rho^+)_{j-\frac{1}{2}} = 0, \tag{2.30}$$

$$\int_{I_j} u\psi dx - \int_{I_j} h^{-1}p\psi dx = \int_{I_j} \widetilde{z}\psi dx, \tag{2.31}$$

$$\int_{I_j} q\phi dx + \int_{I_j} u\phi_x dx - (\widehat{u}\phi^-)_{j+\frac{1}{2}} + (\widehat{u}\phi^+)_{j-\frac{1}{2}} = 0, \tag{2.32}$$

where the numerical fluxes are chosen as

$$\widehat{f}_1 = \{\!\{hu\}\!\} - \frac{\alpha}{2}[\![h]\!], \tag{2.33}$$

$$\widehat{f}_4 = \{\!\{u\widetilde{z} - \frac{1}{2}u^2 + gh - \frac{1}{2}h^2q^2\}\!\} - \frac{\alpha}{2}[\![\widetilde{z}]\!], \tag{2.34}$$

$$\widehat{h^2q} = (h^3q)^-, \quad \widehat{u} = u^+, \tag{2.35}$$

where $\alpha = \max(|u| + \sqrt{gh})$ is the maximum taken in the relevant interval.

2.2.1. Algorithm flowchart (II)

Similar to the fully discrete E_1 conserved scheme, the E_2 conserved scheme coupled with the Euler forward time discretization can be divided in two steps. Given the solution $\mathbf{h^n}, \mathbf{u^n}, \tilde{\mathbf{z}}^\mathbf{n}, \mathbf{p^n}$ and $\mathbf{q^n}$ at the time level t^n, the algorithm can be divided into two steps.

Step I: From the time dependent equations (2.28) and (2.29) with the fluxes (2.33) and (2.34) we have the fully discrete scheme in the matrix form:

$$\frac{\mathbf{h^{n+1}} - \mathbf{h^n}}{\Delta t^n} = \mathbf{res_1}(\mathbf{h^n}, \mathbf{u^n}), \tag{2.36}$$

$$\frac{\tilde{\mathbf{z}}^{\mathbf{n+1}} - \tilde{\mathbf{z}}^\mathbf{n}}{\Delta t^n} = \mathbf{res_4}(\mathbf{h^n}, \mathbf{u^n}, \tilde{\mathbf{z}}^\mathbf{n}, \mathbf{q^n}), \tag{2.37}$$

by the Euler forward method with the time step $\Delta t^n = t^{n+1} - t^n$.

Step II: After we get $\mathbf{h^{n+1}}$ and $\tilde{\mathbf{z}}^{\mathbf{n+1}}$ from the last step, based on the time independent schemes (2.30), (2.31) and (2.32) with the numerical fluxes (2.35), we can solve the corresponding linear system to get $\mathbf{u^{n+1}}, \mathbf{p^{n+1}}, \mathbf{q^{n+1}}$.

Thus we obtain all the numerical solutions at the next time step t^{n+1}.

3. The DG discretization in non-conservative form

In this section, we design and prove a Hamiltonian ($\mathcal{H}$) conserved DG scheme and give its algorithm flowchart.

Combining (1.1) and (1.3) and after some manipulation, we can obtain the Serre equations in the following non-conservative form:

$$h_t + (hu)_x = 0, \tag{3.1}$$

$$hu_t - \beta(h^3u_x)_{xt} + huu_x - \beta(u(h^3u_x)_x)_x + \frac{1}{2}g(h^2)_x - 2\beta(h^3u_x^2)_x = 0. \tag{3.2}$$

Introducing some auxiliary variables m, p, q, s, w, k, v, r,

$$\begin{aligned} m - hu &= 0, \\ p - \frac{1}{2}u^2 &= 0, \\ s - h^3q &= 0, \\ q - u_x &= 0, \\ w - s_x &= 0, \\ k - (hu)_x &= 0, \\ v - \frac{3}{2}h^2qk &= 0, \\ r - \frac{1}{2}h^2qm_x - h^2mq_x - hqmh_x &= 0, \end{aligned} \tag{3.3}$$

the Serre equations can be written as follows:

$$h_t + (hu)_x = 0, \tag{3.4}$$

$$hu_t - \beta w_t + hp_x + \frac{1}{2}g(h^2)_x - \beta(v+r)_x = 0. \tag{3.5}$$

We will introduce the standard L^2 projection operator $\mathbb{P}$ of a function ω into the finite element space V_h, i.e., for all $v \in P^k(I_j)$,

$$\int_{I_j} (\mathbb{P}(\omega) - \omega)v dx = 0, \ \forall j = 1, \cdots, N, \tag{3.6}$$

and define the discrete derivative operator

$$D_j(\omega; \rho) = \int_{I_j} \omega\rho_x dx - (\widehat{\omega}\rho^-)_{j+\frac{1}{2}} + (\widehat{\omega}\rho^+)_{j-\frac{1}{2}},$$

where the numerical flux $\hat{\omega}$ is to be determined. Then for the equations (3.4), (3.5) and the auxiliary equations (3.3), the $\mathcal{H}$ conserved DG scheme can be constructed as follows: Find $h, u, w, q, k, r \in V_h$ such that, for all test functions $\theta, \phi, \zeta, \tau, \gamma, \mu \in V_h$,

$$\int_{I_j} h_t\theta dx - D_j(hu; \theta) = 0, \tag{3.7}$$

$$\int_{I_j} hu_t\phi dx - \beta\int_{I_j} w_t\phi dx + D_j(h\phi; p) - \frac{1}{2}gD_j(h^2; \phi) + \beta D_j(v+r; \phi) = 0, \tag{3.8}$$

$$\int_{I_j} q\tau dx + D_j(u; \tau) = 0, \tag{3.9}$$

$$\int_{I_j} k\gamma dx + D_j(hu; \gamma) = 0, \tag{3.10}$$

$$\int_{I_j} w\zeta dx + D_j(s;\zeta) = 0, \tag{3.11}$$

$$\int_{I_j} r\mu dx - \frac{1}{2} D_j(h^2 q\mu; m) - D_j(h^2 m\mu; q) - D_j(hmq\mu; h) = 0, \tag{3.12}$$

with $m = \mathbb{P}(hu)$, $p = \mathbb{P}(\frac{1}{2}u^2)$, $s = \mathbb{P}(h^3 q)$ and $v = \mathbb{P}(\frac{3}{2}h^2 qk)$ and the numerical fluxes

$$\widehat{hu} = \{\!\{hu\}\!\},\ \widehat{h\phi} = \{\!\{h\phi\}\!\},\ \widehat{h^2} = h^+ h^-, \tag{3.13}$$

$$\widehat{v+r} = v^+ + r^+,\ \widehat{s} = s^+,\ \widehat{u} = u^-, \tag{3.14}$$

$$\widehat{h^2 q\mu} = \{\!\{h^2 q\mu\}\!\},\ \widehat{h^2 m\mu} = \{\!\{h\}\!\}\{\!\{h\mu\}\!\}\{\!\{m\}\!\},\ \widehat{hmq\mu} = \{\!\{h\mu\}\!\}\{\!\{m\}\!\}\{\!\{q\}\!\}. \tag{3.15}$$

Here the choices of the numerical fluxes in the scheme are not unique, which can be seen from the proof of its conservation of Hamiltonian.

3.1. $\mathcal{H}$-stability

In this part, we prove the Hamiltonian conservation of the above scheme. For brevity, we define

$$(v, w) := \sum_{j=1}^{N} \int_{I_j} v w dx,\ D(v; w) := \sum_{j=1}^{N} D_j(v; w). \tag{3.16}$$

Proposition 3.1. *($\mathcal{H}$-stability) The solution to the scheme (3.7)–(3.12) with the numerical fluxes (3.13)–(3.15) satisfies the following $\mathcal{H}$-stability:*

$$\frac{d}{dt}\int_I \frac{1}{2}(hu^2 + gh^2 + \beta h^3 q^2) dx = 0. \tag{3.17}$$

Proof. Summing up the DG schemes (3.7)–(3.12) over j from 1 to N, we have

$$(h_t, \theta) - D(hu; \theta) = 0, \tag{3.18}$$

$$(hu_t, \phi) - \beta(w_t, \phi) + D(h\phi; p) - \frac{1}{2} g D(h^2; \phi) + \beta D(v + r; \phi) = 0, \tag{3.19}$$

$$(w, \zeta) + D(s; \zeta) = 0, \tag{3.20}$$

$$(q, \tau) + D(u; \tau) = 0, \tag{3.21}$$

$$(k, \gamma) + D(hu; \gamma) = 0, \tag{3.22}$$

$$(r, \mu) - D(\frac{1}{2} h^2 q\mu; m) - D(h^2 m\mu; q) - D(hmq\mu; h) = 0. \tag{3.23}$$

By introducing a new auxiliary variable $\nu = \mathbb{P}(\frac{3}{2}h^2 q^2)$ and taking the test functions $\theta = p + gh - \beta\nu$ in (3.18) and $\phi = u$ in (3.19), it follows that

$$(h_t, p + gh - \beta\nu) - D(hu; p + gh - \beta\nu) = 0,$$

$$(hu_t, u) - \beta(w_t, u) + D(hu; p) - \frac{1}{2} g D(h^2; u) + \beta D(v + r; u) = 0.$$

If the following identities hold

$$D(hu; gh) + \frac{1}{2} g D(h^2; u) = 0, \tag{3.24}$$

$$D(hu; \nu) + D(v; u) = 0, \tag{3.25}$$

$$D(r; u) = 0, \tag{3.26}$$

then we have

$$(h_t, p + gh - \beta\nu) + (hu_t, u) - \beta(w_t, u) = 0. \tag{3.27}$$

The equality (3.24) can be obtained easily by substituting the numerical fluxes into it.

To obtain (3.26), by choosing $\tau = r, \mu = q$ in (3.21) and (3.23) and from the identities

$$D(\frac{1}{2}h^2q^2; m) + D(h^2mq; q) + D(hmq^2; h) = 0, \tag{3.28}$$

$$D(r; u) + D(u; r) = 0, \tag{3.29}$$

we can deduce that $(r, q) = 0$ and $D(r; u) = D(u; r) = 0$.

For (3.25), taking $\tau = v$ and $\gamma = \nu$ in (3.21) and (3.22)

$$(q, v) + D(u; v) = 0,$$
$$(k, \nu) + D(hu; \nu) = 0,$$

and the identity

$$D(v; u) + D(u; v) = 0, \tag{3.30}$$

implies that

$$D(hu; \nu) + D(v; u) = -(k, \nu) + (q, v) = -(k, \frac{3}{2}h^2q^2) + (q, \frac{3}{2}h^2qk) = 0.$$

From the time derivative of the equations (3.20) and (3.21) with the test functions $\zeta = u$ and $\tau = s_t$, we have

$$(w_t, u) + D(s_t; u) = 0, \tag{3.31}$$

$$(q, s_t) + D(u; s_t) = 0. \tag{3.32}$$

Thus by the identity

$$D(s_t; u) + D(u; s_t) = 0, \tag{3.33}$$

we get

$$-(w_t, u) = (q, s_t) = (q, (h^3q)_t).$$

Also from

$$(h_t, \nu) = (h_t, \frac{3}{2}h^2q^2),$$

it follows that

$$-\beta(h_t, \nu) - \beta(w_t, u) = \frac{1}{2}\int_I \beta(h^3q^2)_t dx.$$

Similarly we can obtain

$$(h_t, p + gh) + (hu_t, u) = \frac{1}{2}\int_I (hu^2 + gh^2)_t dx.$$

Thus, we see that the equation (3.27) is identical to the (3.17), which completes the proof. □

3.2. Algorithm flowchart (III)

This part displays some details about the implementation for the $\mathcal{H}$ conserved DG scheme. First, we rewrite the semi-discrete scheme into the following vector form as follows:

$$\mathbf{h}_t = \mathbf{res_5}(\mathbf{h}, \boldsymbol{u}), \tag{3.34}$$

$$\mathbf{D}(\mathbf{h})\mathbf{u_t} - \beta\mathbf{w_t} = \mathbf{res_6}(\mathbf{h}, \boldsymbol{u}), \tag{3.35}$$

with $\mathbf{w} = \mathbf{C}(\mathbf{h})\mathbf{u}$ and the matrices $\mathbf{C}(\mathbf{h})$ and $\mathbf{D}(\mathbf{h})$ are the corresponding discrete matrix in the scheme. Notice that there are two equations with three time derivative vectors $\mathbf{h}, \mathbf{u}$ and $\mathbf{w}$. Thus unlike the E_1 and E_2 conserved schemes, the fully discrete $\mathcal{H}$ conserved scheme can not be divided into time dependent and independent parts. Given the solution $\mathbf{h^n}, \mathbf{u^n}$ at time t^n, the forward Euler method can be divided into two steps.

Step I: First, from the equation (3.34), we obtain $\mathbf{h^{n+1}}$ from

$$\frac{\mathbf{h^{n+1}}-\mathbf{h^n}}{\Delta t^n}=\mathbf{res_5}(\mathbf{h^n},\mathbf{u^n}). \tag{3.36}$$

Step II: Then for the equation (3.35), we get $\mathbf{u^{n+1}}$ from

$$\mathbf{D}(\mathbf{h^n})\frac{\mathbf{u^{n+1}}-\mathbf{u^n}}{\Delta t^n}-\beta\frac{\mathbf{C}(\mathbf{h^{n+1}})\mathbf{u^{n+1}}-\mathbf{C}(\mathbf{h^n})\mathbf{u^n}}{\Delta t^n}=\mathbf{res_6}(\mathbf{h^n},\mathbf{u^n}), \tag{3.37}$$

in which we need to solve a global linear system.

For higher order SSP/TVD Runge-Kutta methods, the convex combination of the forward Euler method will be performed on the term ($\mathbf{hu}-\beta\mathbf{w}$) other than $\mathbf{u}$ to get better performance numerically. For example, the second order SSP/TVD Runge-Kutta method is as follows:

$$\frac{\mathbf{h}^*-\mathbf{h^n}}{\Delta t^n}=\mathbf{res_5}(\mathbf{h^n},\mathbf{u^n}), \tag{3.38}$$

$$\mathbf{D}(\mathbf{h^n})\frac{\mathbf{u}^*-\mathbf{u}^n}{\Delta t^n}-\beta\frac{\mathbf{w}^*-\mathbf{w}^n}{\Delta t^n}=\mathbf{res_6}(\mathbf{h^n},\mathbf{u^n}), \tag{3.39}$$

$$\frac{\mathbf{h}^{**}-\mathbf{h}^*}{\Delta t^n}=\mathbf{res_5}(\mathbf{h}^*,\mathbf{u}^*), \tag{3.40}$$

$$\mathbf{D}(\mathbf{h}^*)\frac{\mathbf{u}^{**}-\mathbf{u}^*}{\Delta t^n}-\beta\frac{\mathbf{w}^{**}-\mathbf{w}^*}{\Delta t^n}=\mathbf{res_6}(\mathbf{h}^*,\mathbf{u}^*), \tag{3.41}$$

$$\mathbf{h^{n+1}}=\frac{\mathbf{1}}{\mathbf{2}}\mathbf{h^n}+\frac{\mathbf{1}}{\mathbf{2}}\mathbf{h}^{**}, \tag{3.42}$$

$$\mathbf{D}(\mathbf{h^{n+1}})\mathbf{u^{n+1}}-\beta\mathbf{w^{n+1}}=\frac{\mathbf{1}}{\mathbf{2}}(\mathbf{D}(\mathbf{h^{n+1}})\mathbf{u^n}-\beta\mathbf{w^n})+\frac{\mathbf{1}}{\mathbf{2}}(\mathbf{D}(\mathbf{h^{n+1}})\mathbf{u}^{**}-\beta\mathbf{w}^{**}). \tag{3.43}$$

In the numerical experiments, the similar higher order SSP/TVD Runge-Kutta methods will be used.

4. Numerical results

In this section we present numerical experiments to illustrate the behaviors of the numerical schemes. It is noted that in what follows, we will depict the deviation of the free surface η rather than the total depth h. Several numerical examples with flat bottom can be utilized to check the accuracy and capability. For non-flat bottom situation, we consider to verify the property of well-balanced for the E_1 conserved scheme on different variable bottoms. In order not to cause misunderstanding, we will specific that the notations h, u, η are exact solutions or numerical solutions in each numerical experiment subsequently. Without specific explanations, the CFL condition number is taken as 0.1.

Example 4.1. *(Cnoidal wave solution)*

In this example, we consider to solve cnoidal wave solutions [9] with the periodic boundary condition.

$$h(x,t)=d+\eta,\ u(x,t)=c\Big(1-\frac{h_0}{h(x,t)}\Big),\ \eta=a\mathrm{dn}^2(\kappa(x-ct),m) \tag{4.1}$$

where $\mathrm{dn}(\cdot,m)$ is Jacobian elliptic function with elliptic modulus m. And the parameters are

$$\kappa=\frac{\sqrt{3a}}{2\sqrt{(d+a)(d+(1-k^2)a)}}, \tag{4.2}$$

$$c=\frac{\sqrt{g(d+a)(d+(1-k^2)a)}}{h_0}, \tag{4.3}$$

$$h_0=d+a\frac{E(m)}{K(m)} \tag{4.4}$$

where $K(m)$ and $E(m)$ are the complete elliptic integrals of the first and second kind, respectively [1]. The period is calculated by $T_p=2K(m)/\kappa$. The parameters are given by $d=1.0, a=0.05, g=1.0, \beta=\frac{1}{3}$. The L^2 and L^∞ error orders of the three DG schemes for variables u, h are contained in Tables 4.1, 4.2 and 4.3. For the variable u, all DG schemes have the optimal order of accuracy. For the variable h, the E_1 and E_2 conserved DG scheme still has $(k+1)$-th order of accuracy, however, the $\mathcal{H}$ conserved DG scheme can reach the optimal order of accuracy when $k\geq 2$, only suboptimal order of accuracy when $k=1$. The sketches of cnoidal wave in $[-T_p, T_p]$ are plotted in Fig. 4.1. The efficiency of all three DG schemes is illustrated by CPU time at the terminal time $T=10$ in Table 4.4, from which we can see that the E_2 conserved DG scheme is the most efficient one. Due to more auxiliary variables and special time discretization technique adopted, the $\mathcal{H}$ conserved scheme is much slower.

Table 4.1
Example 4.1, the E_1 conserved scheme for the Serre equations: Cnoidal wave solution with the computational domain $[-T_p, T_p]$, at time $T = 2$. The parameters $d = 0.3, a = 0.1, m = 0.99, g = 9.8$.

	N	$\|e\|_{L^2}$	order	$\|e\|_{L^\infty}$	order	$\|e\|_{L^2}$	order	$\|e\|_{L^\infty}$	order
		u				h			
P^1	80	5.96E-04	–	2.85E-03	–	2.56E-04	–	2.01E-03	–
	160	1.11E-04	2.43	6.45E-04	2.14	6.67E-05	1.94	6.06E-04	1.73
	320	2.41E-05	2.20	1.77E-04	1.87	1.71E-05	1.96	1.66E-04	1.87
	640	5.79E-06	2.06	4.67E-05	1.92	4.31E-06	1.99	4.31E-05	1.95
P^2	80	8.33E-06	–	5.28E-05	–	7.83E-06	–	6.63E-05	–
	160	1.16E-06	2.85	9.07E-06	2.54	1.28E-06	2.62	9.89E-06	2.75
	320	1.29E-07	3.16	1.03E-06	3.14	1.65E-07	2.95	1.54E-06	2.68
	640	1.52E-08	3.09	1.25E-07	3.05	1.99E-08	3.05	1.91E-07	3.01
P^3	80	3.36E-07	–	1.65E-06	–	4.57E-07	–	2.27E-06	–
	160	1.16E-08	4.85	8.26E-08	4.32	1.51E-08	4.92	1.04E-07	4.45
	320	7.15E-10	4.02	5.35E-09	3.95	9.59E-10	3.97	6.67E-09	3.96
	640	4.47E-11	4.00	3.39E-10	3.98	4.78E-11	4.33	4.19E-10	3.99

Table 4.2
Example 4.1, the E_2 conserved DG scheme for the Serre equations: Cnoidal wave solution with the computational domain $[-T_p, T_p]$, at time $T = 2$. The parameters $d = 0.3, a = 0.1, m = 0.99, g = 9.8$.

	N	$\|e\|_{L^2}$	order	$\|e\|_{L^\infty}$	order	$\|e\|_{L^2}$	order	$\|e\|_{L^\infty}$	order
		u				h			
P^1	80	6.38E-04	–	3.49E-03	–	2.57E-04	–	2.10E-03	–
	160	1.08E-04	2.56	6.36E-04	2.46	6.49E-05	1.99	5.68E-04	1.89
	320	2.02E-05	2.42	1.39E-04	2.20	1.64E-05	1.98	1.58E-04	1.85
	640	4.50E-06	2.17	3.84E-05	1.85	4.15E-06	1.99	4.12E-05	1.94
P^2	80	6.97E-06	–	4.64E-05	–	5.91E-06	–	4.21E-05	–
	160	9.92E-07	2.81	8.07E-06	2.52	1.14E-06	2.38	9.52E-06	2.14
	320	1.21E-07	3.03	1.00E-06	3.01	1.73E-07	2.71	1.56E-06	2.61
	640	1.50E-08	3.02	1.23E-07	3.02	2.14E-08	3.02	1.97E-07	2.99
P^3	80	2.94E-07	–	1.46E-06	–	3.78E-07	–	1.77E-06	–
	160	1.18E-08	4.64	8.66E-08	4.07	1.30E-08	4.86	1.13E-07	3.97
	320	7.19E-10	4.04	5.37E-09	4.01	7.79E-10	4.06	6.48E-09	4.12
	640	4.48E-11	4.01	3.35E-10	4.00	4.64E-11	4.07	4.03E-10	4.01

Table 4.3
Example 4.1, the $\mathcal{H}$ conserved DG scheme for the Serre equations: Cnoidal wave solution with the computational domain $[-T_p, T_p]$, at time $T = 2$. The parameters $d = 0.3, a = 0.1, m = 0.99, g = 9.8$.

	N	$\|e\|_{L^2}$	order	$\|e\|_{L^\infty}$	order	$\|e\|_{L^2}$	order	$\|e\|_{L^\infty}$	order
		u				h			
P^1	80	1.78E-03	–	8.12E-03	–	9.32E-04	–	4.84E-03	–
	160	3.85E-04	2.21	1.77E-03	2.19	5.65E-04	0.72	3.70E-03	0.39
	320	8.94E-05	2.11	4.30E-04	2.04	3.17E-04	0.83	1.86E-03	0.99
	640	2.23E-05	2.00	1.07E-04	2.01	1.67E-04	0.93	1.00E-03	0.89
P^2	80	4.52E-04	–	2.09E-03	–	1.16E-04	–	7.21E-04	–
	160	5.74E-05	2.98	2.61E-04	3.01	1.39E-05	3.06	7.41E-05	3.28
	320	7.26E-06	2.98	3.25E-05	3.00	1.69E-06	3.04	8.65E-06	3.10
	640	9.21E-07	2.98	4.00E-06	3.02	2.16E-07	2.97	1.06E-06	3.02
P^3	80	5.36E-05	–	2.40E-04	–	1.22E-05	–	6.31E-05	–
	160	3.40E-06	3.98	1.49E-05	4.01	7.80E-07	3.97	3.99E-06	3.98
	320	2.20E-07	3.95	9.31E-07	4.00	5.22E-08	3.90	2.66E-07	3.91
	640	1.56E-08	3.81	6.88E-08	3.76	3.87E-09	3.76	1.85E-08	3.85

Table 4.4
Example 4.1, CPU time of proposed LDG schemes: Cnoidal wave solution with $N = 160$ cells in computational domain $[-T_p, T_p]$, at time $T = 10$. The parameters $d = 0.3, a = 0.1, m = 0.99, g = 9.8$.

	E_1 conserved scheme	E_2 conserved scheme	$\mathcal{H}$ conserved scheme
P^1	5.02	4.08	29.56
P^2	12.17	9.67	63.69

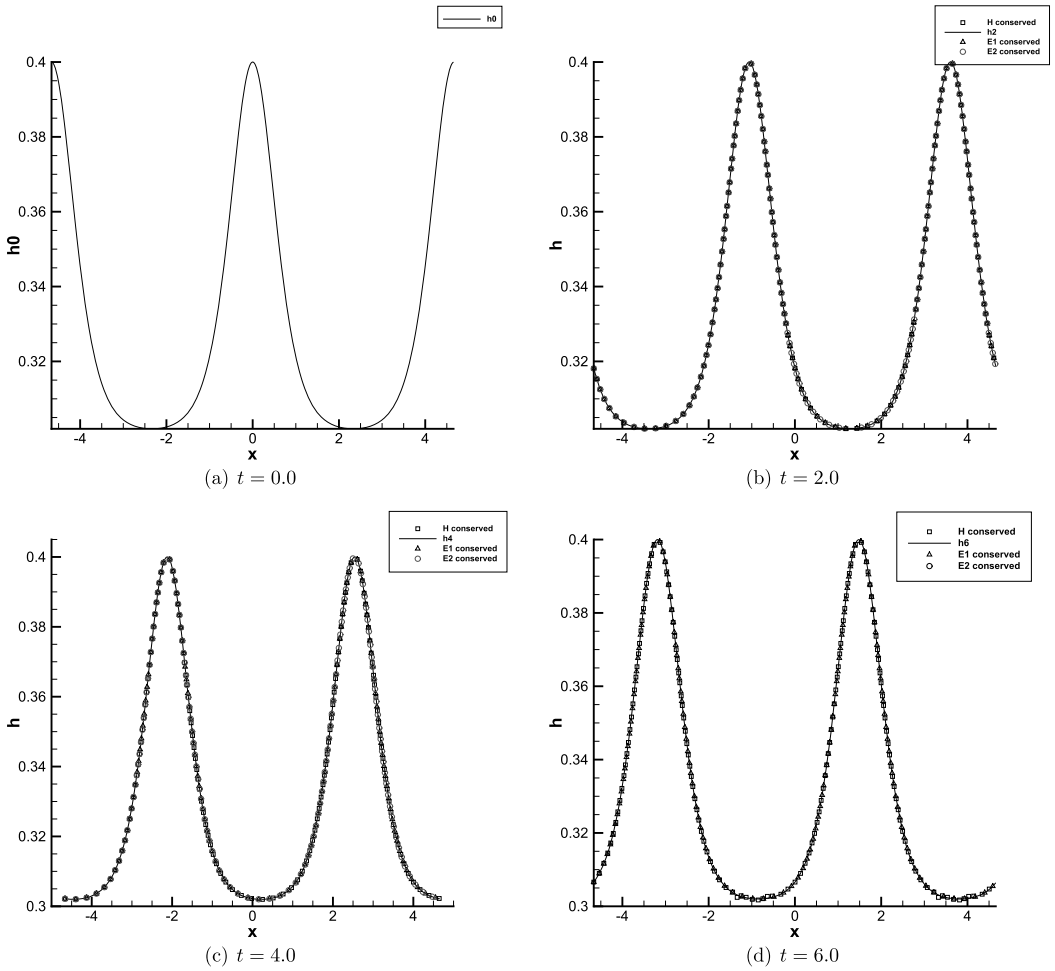

Fig. 4.1. Example 4.1, cnoidal wave solution with the computational domain $[-T_p, T_p]$, $N = 160$ cells, P^2 elements. The parameters $d = 0.3, a = 0.1, m = 0.99, g = 9.8$.

Example 4.2. *(Head-on collision)*

In this example, we study the symmetric head-on collision of two solitary waves moving in opposite directions. There is no analytical solution for this problem because these waves do not retain their shapes after collision. We give the initial values which are two solitary waves located at $x_0 = \pm 20$ with the same amplitude $a_1 = a_2 = 0.15$. Due to the exponential decay of the solution, we adopt the periodic boundary condition in computational domain $[-40, 40]$ with $N = 1000$ uniform cells. The parameters are $d = 1.0, g = 1.0, \beta = \frac{1}{3}$. In Fig. 4.2, the process of interaction between two solitary waves is displayed. These two solitary waves collide quasi-elastically and continue to propagate in opposite directions after the interaction. At time $T \approx 18.84$, the maximum value of amplitude (so called run-up value) is larger than the sum of the amplitudes of the two initial solitary waves. After head-on collision, two solitary waves with different amplitudes are separated and the amplitudes become $a_1 \approx 0.1490, a_2 \approx 0.1486$, compared with the initial amplitudes $a_1 = a_2 = 0.15$. And some small wavelets between two solitary waves shown in Fig. 4.2 (f) clearly indicate that the collision is inelastic.

Example 4.3. *(Overtaking collision)*

This example is devoted to show the overtaking collision of two different amplitude solitary waves. Initially, two solitary waves are located at $x_1 = -60$ with the larger amplitude $a_1 = 0.6$ and $x_2 = -45$ with the smaller amplitude $a_2 = 0.1$. The rest parameters are given by $d = 1.0, g = 1.0, \beta = \frac{1}{3}$. And the these two waves will travel in the same direction with different speeds. The computational domain is $[-75, 75]$ with $N = 1000$ uniform cells. As shown in Fig. 4.3, there is a symmetric, unimodal conglomerate at the peak of interaction at time $T = 50, 65$. The small solitary wave is absorbed by the large solitary wave completely. Following this, the smaller solitary wave is ejected behind the larger wave and propagates independently. Compared with the head-on collision case, the overtaking collision is referred as a strong interaction of solitary waves due to the relative importance of nonlinearity [28]. And this interaction is also inelastic due to the small dispersive tails emerging after the over-taking collision.

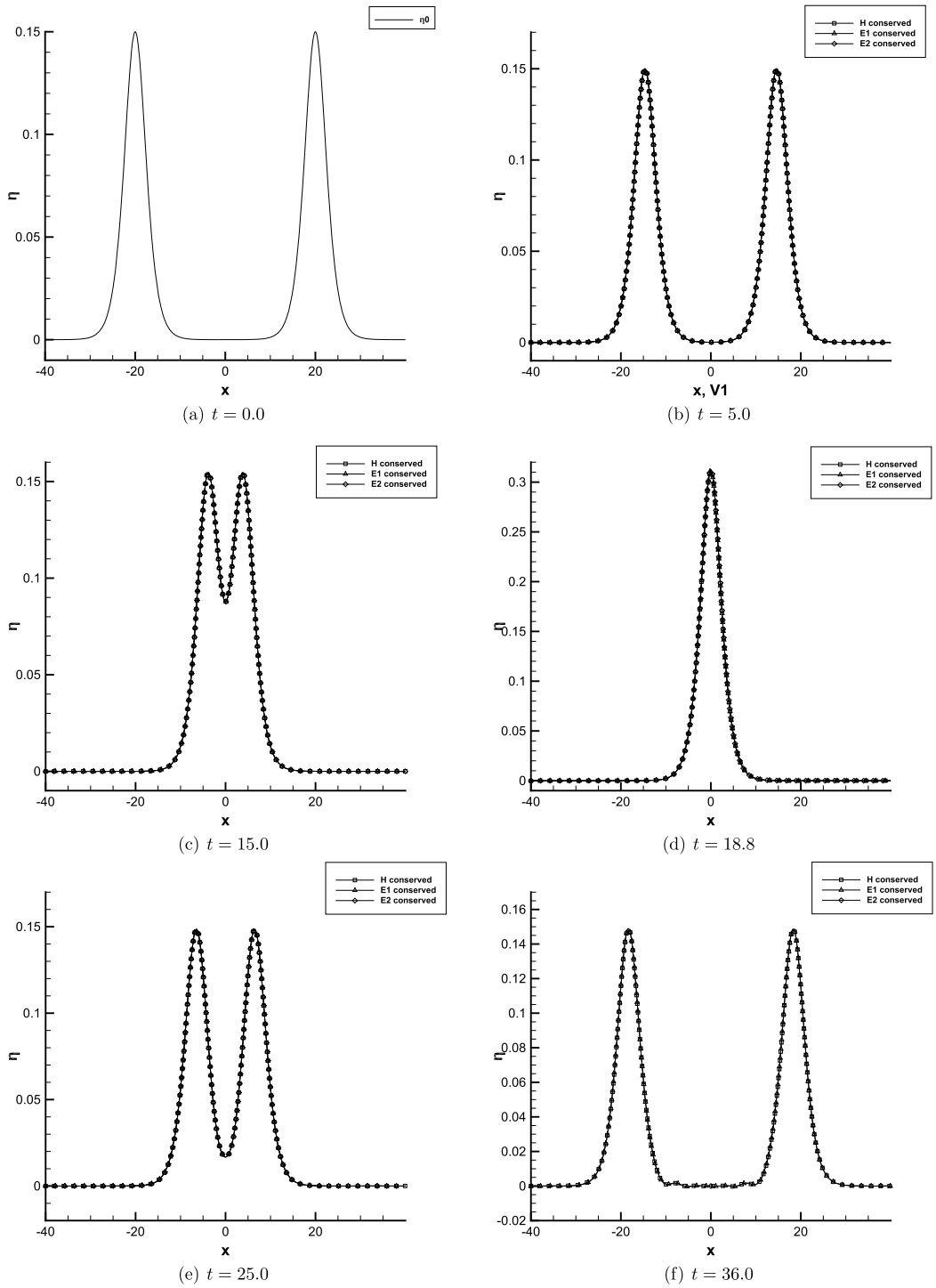

(a) $t = 0.0$ (b) $t = 5.0$

(c) $t = 15.0$ (d) $t = 18.8$

(e) $t = 25.0$ (f) $t = 36.0$

Fig. 4.2. Example 4.2, head-on collision with $N = 1000$ cells, P^3 elements.

Example 4.4. *(Breakup of a Gaussian hump)*

In this example, we take the initial conditions as a heap of water,

$$\eta_0(x) = e^{\frac{-x^2}{10}},\ u_0 = 0, \tag{4.5}$$

which represent a Gaussian hump initially. It will break up into two solitary waves and some small dispersive tails. These waves and their dispersive tails travel in opposite directions. The process is shown in Fig. 4.4. Compared with the results

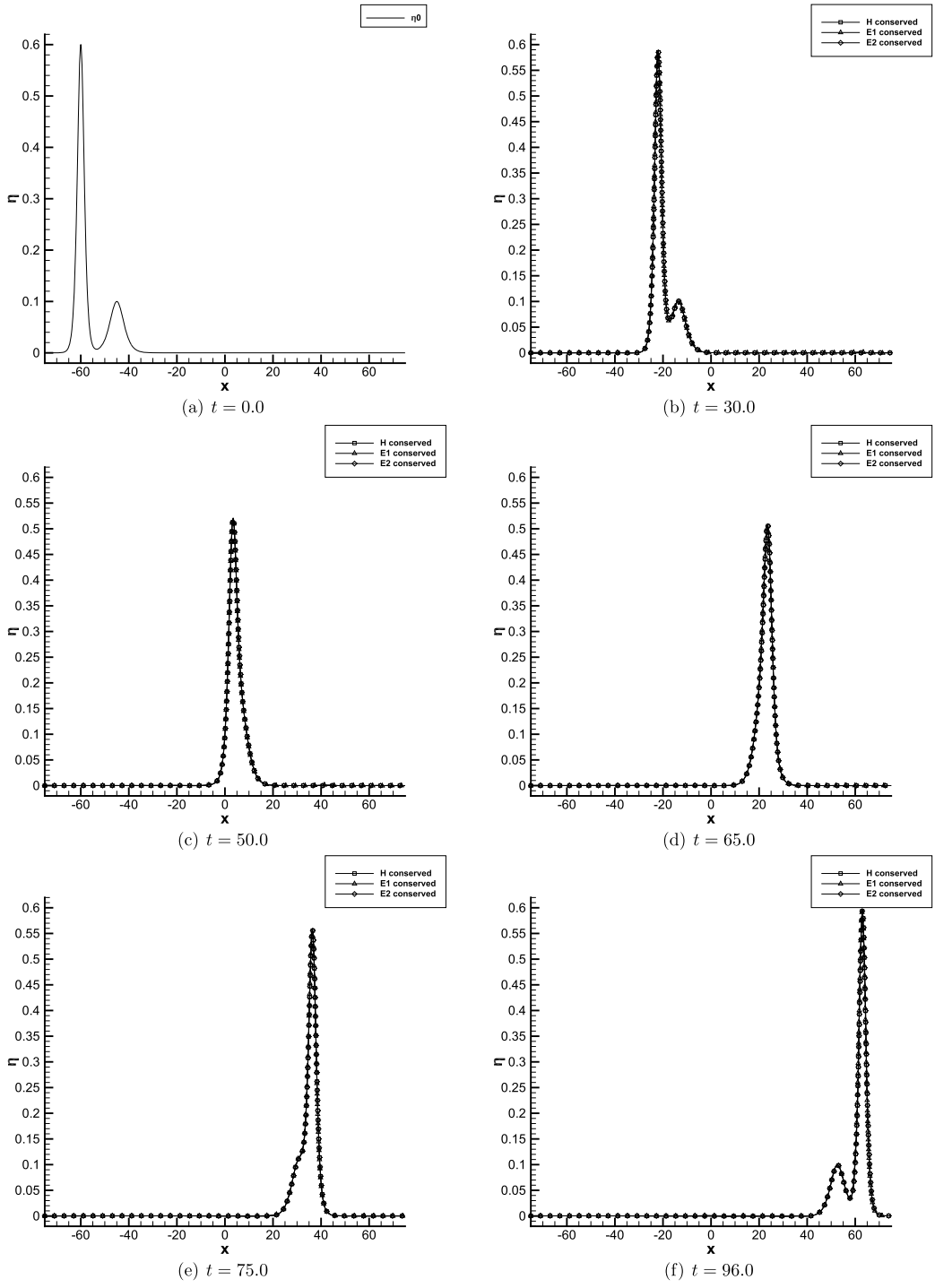

(a) $t = 0.0$ (b) $t = 30.0$

(c) $t = 50.0$ (d) $t = 65.0$

(e) $t = 75.0$ (f) $t = 96.0$

Fig. 4.3. Example 4.3, overtaking collision with $N = 1000$ cells, P^3 elements.

in [30], our numerical schemes resolve this problem well. The CFL ratio can be taken as 0.5 to guarantee the numerical stability of our numerical schemes.

Example 4.5. *(Dispersive shock wave)*

In the shallow water system, when the dissipation can be ignored compared with the dispersive effects, it will emerge dispersive shock wave, which changes rapidly and monotonically in the flow properties. The dispersive shock wave attracted

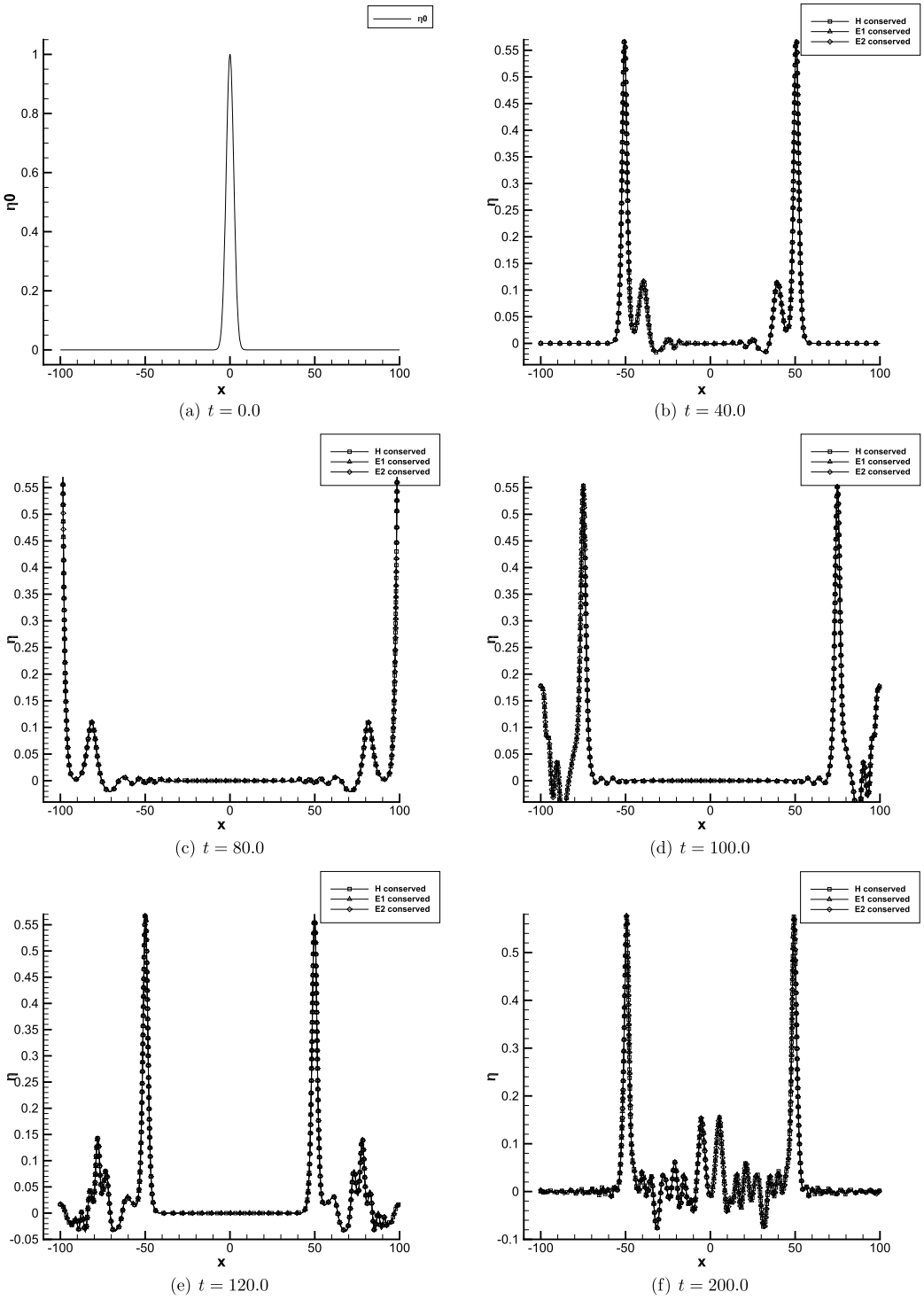

Fig. 4.4. Example 4.4, breakup of a Gaussian hump with $N = 1000$ cells, P^3 elements.

much interest and been well studies in [20,19,21]. We will approximate this wave to test our three numerical scheme in this example. The initial data for exact solutions h, u are taken as step functions

$$h(x,0) = 1 + \frac{1}{2}\eta_0[1 + \tanh(250 - |x|)], \tag{4.6}$$

$$u(x,0) = 2[\sqrt{h(x,0)} - 1], \tag{4.7}$$

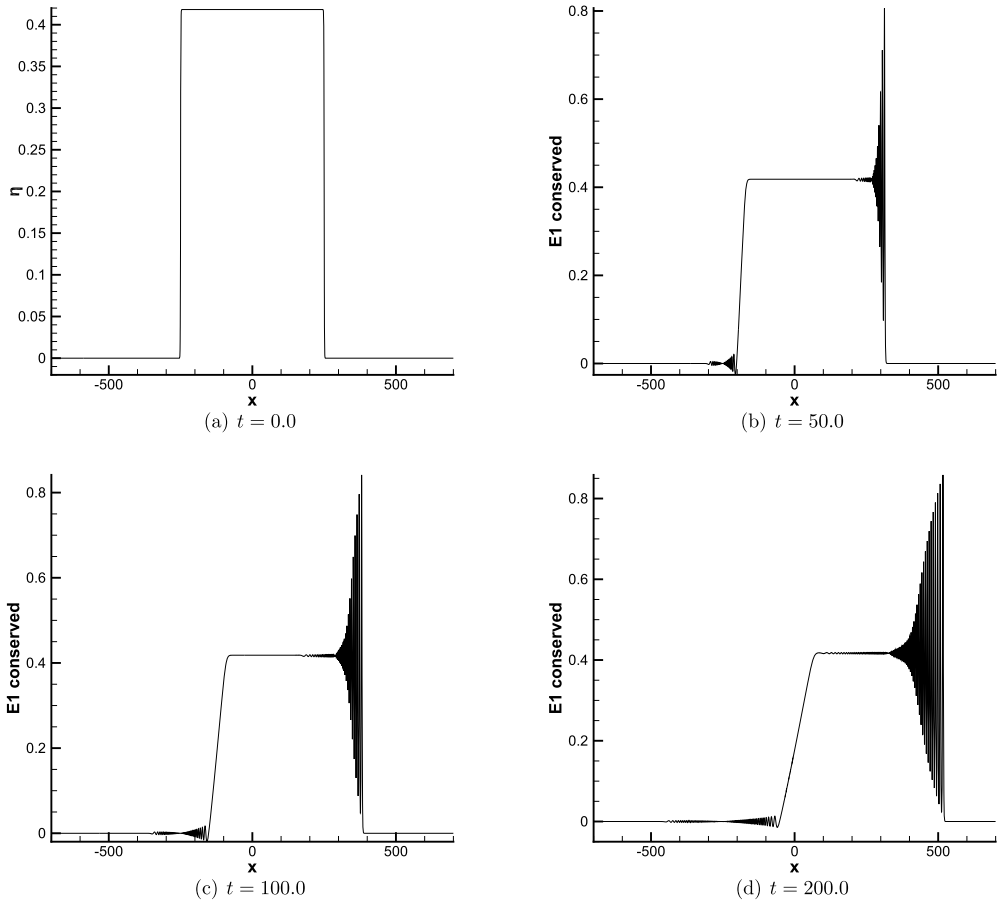

(a) $t = 0.0$ (b) $t = 50.0$ (c) $t = 100.0$ (d) $t = 200.0$

Fig. 4.5. Example 4.5, the E_1 conserved DG scheme for dispersive shock wave with $N = 3000$ cells, P^3 elements.

where $\eta_0 = 0.4182$. Figs. 4.5, 4.6 and 4.7 shows the simulation at time $T = 0, 50, 100, 200$ for the E_1, E_2 and $\mathcal{H}$ conserved DG schemes, respectively. Without introducing spurious oscillations, it is clearly seen that a simple dispersive wave is generated and travel to the right, in the meantime, there is a rarefaction wave travel to the left with a small dispersive tail. At time $T = 200$, the amplitude of the leading edge solitary wave is approximately 0.8585 to 0.8589 at point $x \approx 516.6$, which validate the high accuracy and non-dissipativity of these three numerical scheme, compared with [30].

Example 4.6. *(Validation of well-balance property)*

This example with variable bottoms is used to verify the property of well-balanced for the E_1 conserved DG scheme which we mentioned in Section 2.1. A smooth variable bottom

$$d(x) = -0.5 + (x - 0.5)^2, \tag{4.8}$$

and discontinuous variable bottom

$$d(x) = \begin{cases} -0.5, & 0.3 \le x \le 0.7, \\ 0, & \text{otherwise}, \end{cases} \tag{4.9}$$

are adopted in computational domain $[0, 1]$, respectively, The initial condition for variables (η, u) are

$$\eta = h - d = 1, \quad u = 0. \tag{4.10}$$

For comparison with the results in [25], we give the L^1 and L^∞ errors between numerical solution $(h, hu)|_{T=0.5}$ and the initial data $(h_0, h_0 u_0)$ with $N = 50$ cells in Table 4.5. The error can arrive the order of machine error which guarantee the well-balanced property. The still-water stationary solutions are plotted in Fig. 4.8. Here, we use (H, U) denote the exact solution and (h, u) denote the numerical solution to distinguish. We can see that the stationary solution is well preserved whether the bottom is smooth or not.

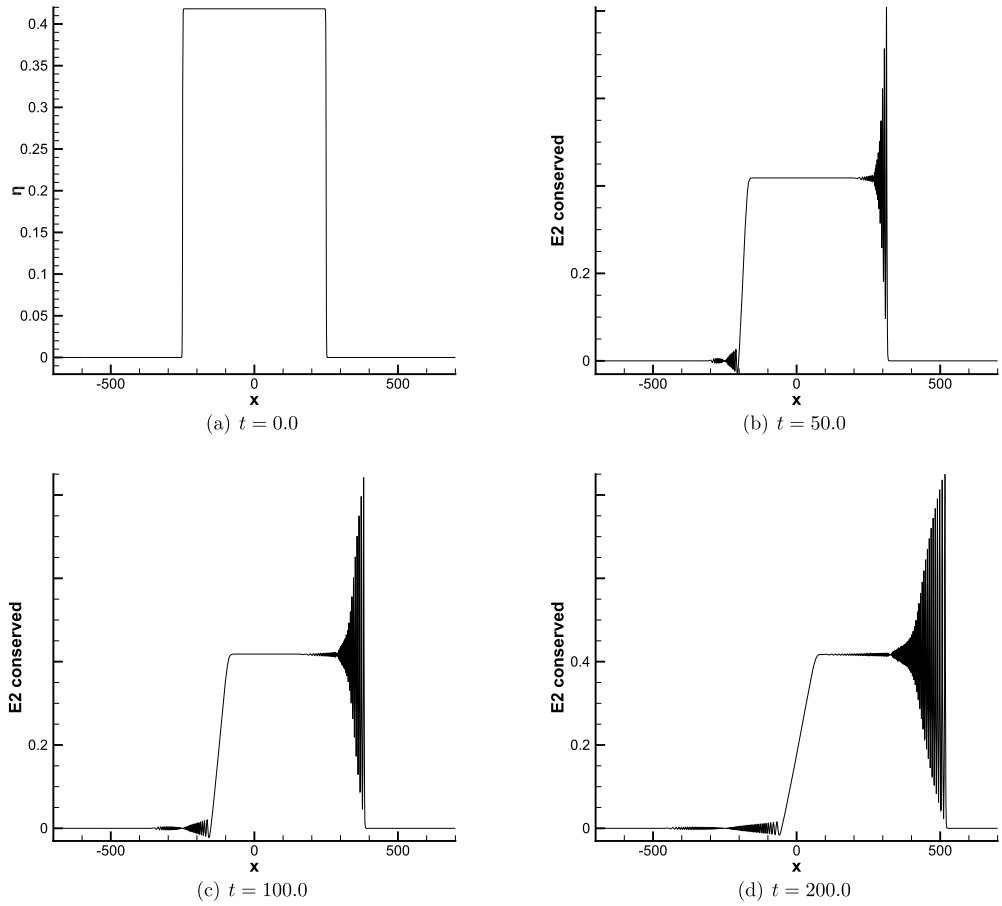

(a) $t = 0.0$ (b) $t = 50.0$

(c) $t = 100.0$ (d) $t = 200.0$

Fig. 4.6. Example 4.5, the E_2 conserved DG scheme for dispersive shock wave with $N = 3000$ cells, P^3 elements.

Table 4.5
Example 4.6, L^1 and L^∞ errors for variables (h, hu) at $T = 0.5$, P^2 elements.

	$\|h - h_0\|_{L^1}$	$\|h - h_0\|_{L^\infty}$	$\|hu - h_0u_0\|_{L^1}$	$\|hu - h_0u_0\|_{L^\infty}$
smooth bottom	6.93E-16	9.21E-15	1.40E-15	1.20E-14
discontinuous bottom	7.98E-16	4.75E-14	5.78E-15	4.12E-15

5. Conclusion

We designed three numerical schemes for the Serre equations under the DG framework. The forms of conservation laws were adopted for the development E_1 or E_2 conserved schemes. For the non-flat bottom situation, the E_1 conserved scheme was modified to preserve exactly well-balanced property. The $\mathcal{H}$ conserved scheme was constructed based on the equations in nonconservative form successfully.

Furthermore, a series of numerical experiments were given to validate our methods. The cnoidal wave examples show that all numerical schemes are highly accurate and stable. To be more specific, for the variable u, all DG schemes can achieve the optimal order of accuracy. For the variable h, the E_1 and E_2 conserved schemes maintain the optimal order of accuracy, while the $\mathcal{H}$ conserved scheme can reach the optimal order of convergence rate when $k \geq 2$, but only suboptimal order of accuracy when $k = 1$. In order to demonstrate the robustness and effectiveness, we have applied these schemes on the interaction of solitary waves, the breakup of a Gaussian hump, and the dispersive shock wave problems of the shallow water model. From the contrastive experimental figures, we can see that all three conserved schemes proposed in this paper are successfully validated.

The E_1 and E_2 conserved schemes can be extended to the two-dimensional problem directly. Since the non-conservative form and more unknown variables are involved in the Hamiltonian conserved scheme, the two-dimensional $\mathcal{H}$ conserved scheme and numerical comparisons will be presented in our future work.

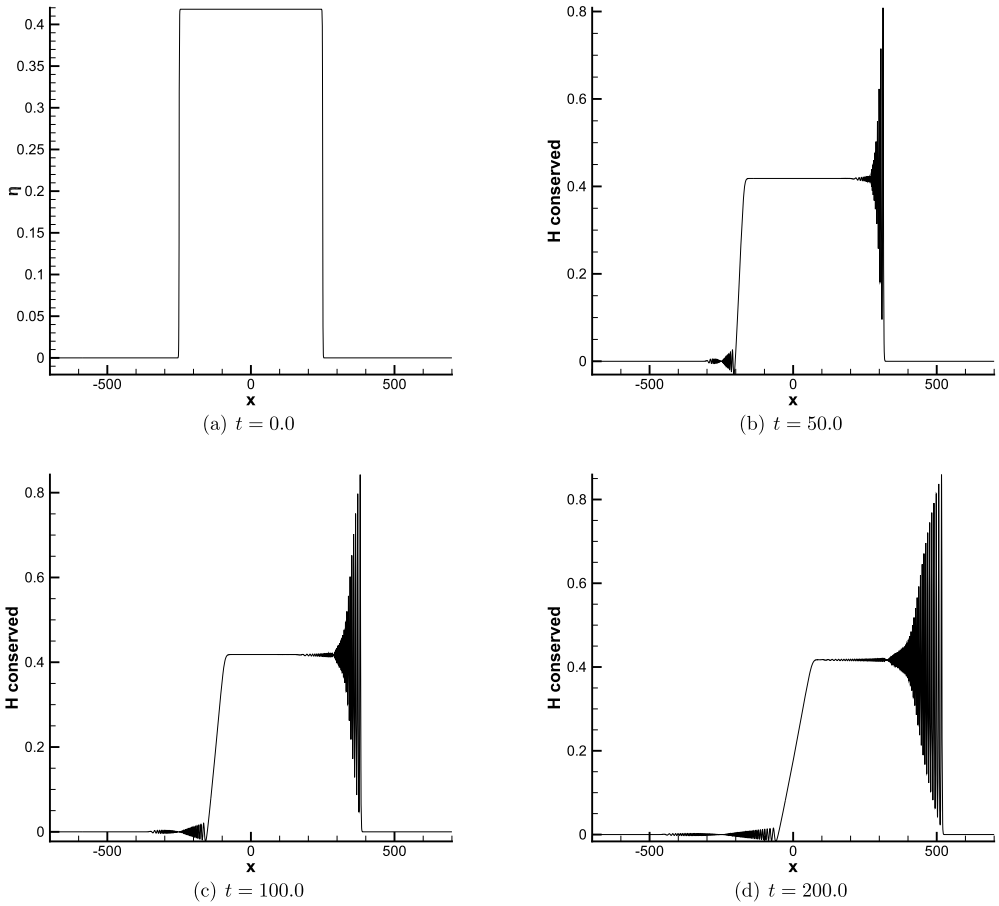

Fig. 4.7. Example 4.5, the $\mathcal{H}$ conserved DG scheme for dispersive shock wave with $N = 3000$ cells, P^2 elements.

CRediT authorship contribution statement

Jianli Zhao: Methodology, Software, Writing - original draft, Writing - review & editing. **Qian Zhang:** Methodology, Software, Validation, Writing - review & editing. **Yang Yang:** Conceptualization, Methodology, Writing - review & editing. **Yinhua Xia:** Conceptualization, Methodology, Writing - review & editing.

Declaration of competing interest

The authors declare that they have no known competing financial interests or personal relationships that could have appeared to influence the work reported in this paper.

References

[1] M. Abramowitz, I.A. Stegun, Handbook of Mathematical Functions: With Formulas, Graphs, and Mathematical Tables, vol. 55, Courier Corporation, 1965.
[2] J.S. Antunes Do Carmo, Boussinesq and Serre type models with improved linear dispersion characteristics applications, J. Hydraul. Res. 51 (6) (2013) 719–727.
[3] E. Barthélemy, Nonlinear shallow water theories for coastal waves, Surv. Geophys. 25 (3–4) (2004) 315–337.
[4] F. Bassi, S. Rebay, A high-order accurate discontinuous finite element method for the numerical solution of the compressible Navier–Stokes equations, J. Comput. Phys. 131 (2) (1997) 267–279.
[5] A. Bermudez, M.E. Vázquez, Upwind methods for hyperbolic conservation laws with source terms, Comput. Fluids 23 (8) (1994) 1049–1071.
[6] J. Bona, H. Chen, O. Karakashian, Y. Xing, Conservative, discontinuous Galerkin–methods for the generalized Korteweg–de Vries equation, Math. Comput. 82 (283) (2013) 1401–1432.
[7] P. Bonneton, E. Barthélemy, F. Chazel, R. Cienfuegos, D. Lannes, F. Marche, M. Tissier, Recent advances in Serre–Green Naghdi modelling for wave transformation, breaking and runup processes, Eur. J. Mech. B, Fluids 30 (6) (2011) 589–597.
[8] P. Bonneton, F. Chazel, D. Lannes, F. Marche, M. Tissier, A splitting approach for the fully nonlinear and weakly dispersive Green–Naghdi model, J. Comput. Phys. 230 (4) (2011) 1479–1498.
[9] J.D. Carter, R. Cienfuegos, The kinematics and stability of solitary and cnoidal wave solutions of the Serre equations, Eur. J. Mech. B, Fluids 30 (3) (2011) 259–268.

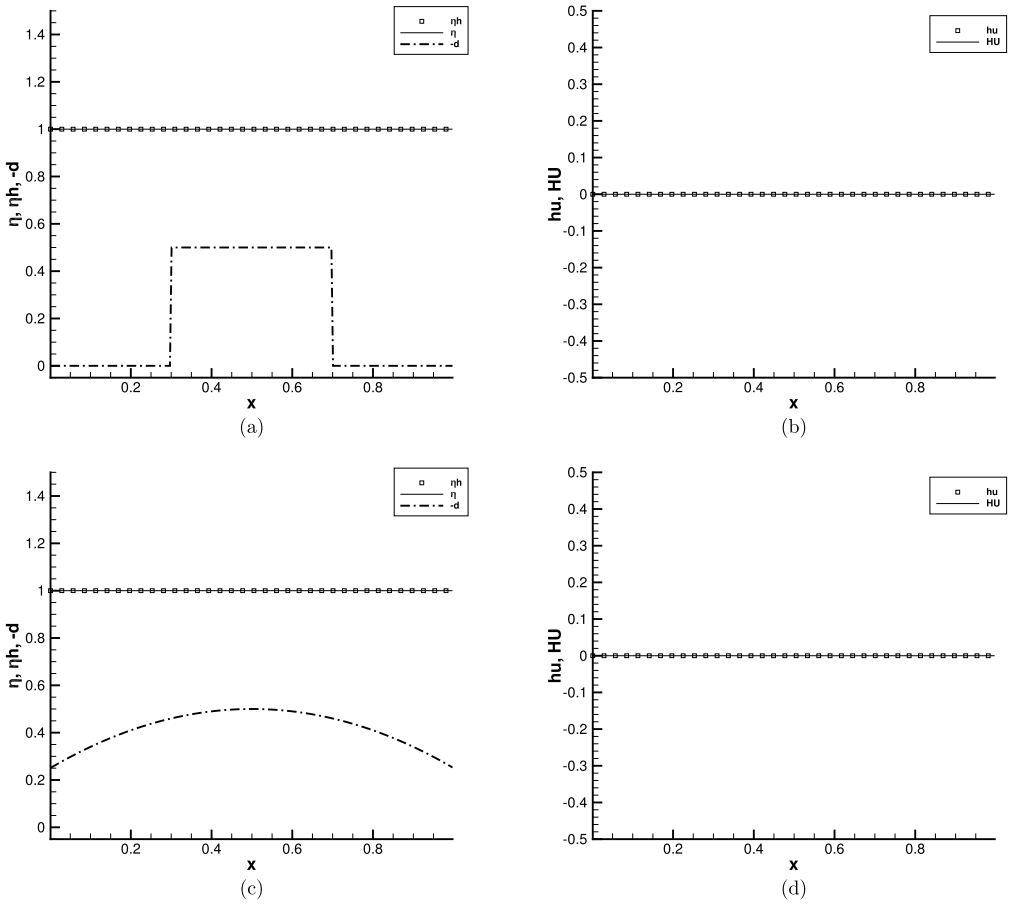

Fig. 4.8. Example 4.6, numerical simulations at $T = 0.5$ for well-balanced property of the E_1 conserved DG scheme with $N = 50$ cells, P^2 elements.

[10] Y. Cheng, C.-W. Shu, A discontinuous Galerkin finite element method for directly solving the Hamilton–Jacobi equations, J. Comput. Phys. 223 (1) (2007) 398–415.
[11] B. Cockburn, Discontinuous Galerkin methods for convection-dominated problems, in: High-order Methods for Computational Physics, 1999, pp. 69–224.
[12] B. Cockburn, C.-W. Shu, TVB Runge-Kutta local projection discontinuous Galerkin finite element method for conservation laws. II. General framework, Math. Comput. 52 (186) (1989) 411–435.
[13] B. Cockburn, C.-W. Shu, Runge–Kutta discontinuous Galerkin methods for convection-dominated problems, J. Sci. Comput. 16 (3) (2001) 173–261.
[14] B. Cockburn, C.-W. Shu, Foreword for the special issue on discontinuous Galerkin method, J. Sci. Comput. 22 (23) (2005) 1–3.
[15] C. Dawson, Foreword for the special issue on discontinuous Galerkin method, Comput. Methods Appl. Mech. Eng. 195 (2006) 3183.
[16] F. Dias, P. Milewski, On the fully nonlinear shallow water generalized Serre equations, Phys. Lett. A 374 (8) (2010) 1049–1053.
[17] A. Duran, F. Marche, A discontinuous Galerkin method for a new class of Green-Naghdi equations on simplicial unstructured meshes, Appl. Math. Model. 45 (2017) 840–864.
[18] D. Dutykh, D. Clamond, P. Milewski, D. Mitsotakis, Finite volume and pseudo-spectral schemes for the fully nonlinear 1D Serre equations, Eur. J. Appl. Math. 24 (5) (2013) 761–787.
[19] G. El, R. Grimshaw, N. Smyth, Asymptotic description of solitary wave trains in fully nonlinear shallow-water theory, Physica D 237 (19) (2008) 2423–2435.
[20] G. El, R.H. Grimshaw, N.F. Smyth, Unsteady undular bores in fully nonlinear shallow-water theory, Phys. Fluids 18 (2) (2006) 027104.
[21] J. Esler, J. Pearce, Dispersive dam-break and lock-exchange flows in a two-layer fluid, J. Fluid Mech. 667 (2011) 555–585.
[22] A.E. Green, N. Laws, P. Naghdi, On the theory of water waves, Proc. R. Soc. Lond. Ser. A, Math. Phys. Sci. 338 (1612) (1974) 43–55.
[23] A.E. Green, P.M. Naghdi, A derivation of equations for wave propagation in water of variable depth, J. Fluid Mech. 78 (2) (1976) 237–246.
[24] D. Lannes, P. Bonneton, Derivation of asymptotic two-dimensional time-dependent equations for surface water wave propagation, Phys. Fluids 21 (1) (2009) 016601.
[25] M. Li, P. Guyenne, F. Li, L. Xu, High order well-balanced CDG–FE methods for shallow water waves by a Green–Naghdi model, J. Comput. Phys. 257 (2014) 169–192.
[26] Y.A. Li, J.M. Hyman, W. Choi, A numerical study of the exact evolution equations for surface waves in water of finite depth, Stud. Appl. Math. 113 (3) (2004) 303–324.
[27] H. Liu, N. Yi, A Hamiltonian preserving discontinuous Galerkin method for the generalized Korteweg–de Vries equation, J. Comput. Phys. 321 (2016) 776–796.
[28] J.W. Miles, Obliquely interacting solitary waves, J. Fluid Mech. 79 (1) (1977) 157–169.
[29] R.M. Mirie, C. Su, Collisions between two solitary waves. Part 2. A numerical study, J. Fluid Mech. 115 (1982) 475–492.
[30] D. Mitsotakis, B. Ilan, D. Dutykh, On the Galerkin/finite-element method for the Serre equations, J. Sci. Comput. 61 (1) (2014) 166–195.

[31] N. Panda, C. Dawson, Y. Zhang, A.B. Kennedy, J.J. Westerink, A.S. Donahue, Discontinuous Galerkin methods for solving Boussinesq-Green-Naghdi equations in resolving non-linear and dispersive surface water waves, J. Comput. Phys. 273 (2014) 572–588.
[32] S. Qian, G. Li, F. Shao, Y. Xing, Positivity-preserving well-balanced discontinuous Galerkin methods for the shallow water flows in open channels, Adv. Water Resour. 115 (2018) 172–184.
[33] W.H. Reed, T. Hill, Triangular mesh methods for the neutron transport equation, Los Alamos Scientific Lab., N. Mex. (USA), 1973.
[34] A. Samii, C. Dawson, An explicit hybridized discontinuous Galerkin method for Serre-Green-Naghdi wave model, Comput. Methods Appl. Mech. Eng. 330 (2018) 447–470.
[35] F.J. Seabra-Santos, D.P. Renouard, A.M. Temperville, Numerical and experimental study of the transformation of a solitary wave over a shelf or isolated obstacle, J. Fluid Mech. 176 (1987) 117–134.
[36] F. Serre, Contribution àl'étude des écoulements permanents et variables dans les canaux, La Houille Blanche 6 (1953) 830–872.
[37] C.-W. Shu, Total-variation-diminishing time discretizations, SIAM J. Sci. Stat. Comput. 9 (6) (1988) 1073–1084.
[38] C.-W. Shu, S. Osher, Efficient implementation of essentially non-oscillatory shock-capturing schemes, J. Comput. Phys. 77 (2) (1988) 439–471.
[39] C.H. Su, C.S. Gardner, Korteweg-de Vries equation and generalizations. III. Derivation of the Korteweg-de Vries equation and Burgers equation, J. Math. Phys. 10 (3) (1969) 536–539.
[40] G.B. Whitham, Linear and Nonlinear Waves, vol. 42, John Wiley and Sons, 2011.
[41] Y. Xia, Y. Xu, A conservative local discontinuous Galerkin method for the Schrödinger-KdV system, Commun. Comput. Phys. 15 (4) (2014) 1091–1107.
[42] Y. Xia, Y. Xu, C.-W. Shu, Local discontinuous Galerkin methods for the generalized Zakharov system, J. Comput. Phys. 229 (4) (2010) 1238–1259.
[43] Y. Xu, C.-W. Shu, Local discontinuous Galerkin methods for three classes of nonlinear wave equations, J. Comput. Math. 22 (2) (2004) 250–274.
[44] Y. Xu, C.-W. Shu, Local discontinuous Galerkin methods for nonlinear Schrödinger equations, J. Comput. Phys. 205 (1) (2005) 72–97.
[45] Y. Xu, C.-W. Shu, Local discontinuous Galerkin methods for two classes of two-dimensional nonlinear wave equations, Physica D 208 (1–2) (2005) 21–58.
[46] Y. Xu, C.-W. Shu, Local discontinuous Galerkin methods for the Kuramoto–Sivashinsky equations and the Ito-type coupled KdV equations, Comput. Methods Appl. Mech. Eng. 195 (2006) 3430–3447.
[47] Y. Xu, C.-W. Shu, A local discontinuous Galerkin method for the Camassa–Holm equation, SIAM J. Numer. Anal. 46 (4) (2008) 1998–2021.
[48] Y. Xu, C.-W. Shu, Local discontinuous Galerkin methods for high-order time-dependent partial differential equations, Commun. Comput. Phys. 7 (1) (2010) 1–46.
[49] J. Yan, C.-W. Shu, A local discontinuous Galerkin method for KdV type equations, SIAM J. Numer. Anal. 40 (2) (2002) 769–791.
[50] J. Yan, C.-W. Shu, Local discontinuous Galerkin methods for partial differential equations with higher order derivatives, J. Sci. Comput. 17 (1) (2002) 27–47.
[51] C. Zhang, Y. Xu, Y. Xia, Local discontinuous Galerkin methods for the μ-Camassa–Holm and μ-Degasperis–Procesi equations, J. Sci. Comput. 79 (2) (2019) 1294–1334.
[52] Q. Zhang, Y. Xia, Conservative and dissipative local discontinuous Galerkin methods for Korteweg-de Vries type equations, Commun. Comput. Phys. 25 (2) (2019) 532–563.
[53] Q. Zhang, Y. Xia, Discontinuous Galerkin methods for short pulse type equations via hodograph transformations, J. Comput. Phys. 399 (2019) 108928.